Control of redundant robot arms with null-space compliance and singularity-free orientation representation

Fabio Vigoriti[a], Fabio Ruggiero[a,*], Vincenzo Lippiello[a], Luigi Villani[a]

[a] *Consorzio CREATE and PRISMA Lab, Department of Electrical Engineering and Information Technology, University of Naples, via Claudio 21, 80125, Naples, Italy.*

Abstract

This paper tackles the problem of controlling the position and orientation, expressed in a singularity-free representation form, of the end-effector of a redundant robot, while addressing an active compliant behaviour within the null-space. The manuscript extends the work in [1] by explicitly addressing the orientation part. In order to successfully accomplish the task, a dynamic controller is designed without need of any exteroceptive sensors information. A rigorous stability analysis is provided to confirm the developed theory. Experiments are finally carried out to bolster the performance of the proposed approach.

Keywords: redundant robots, null-space compliance, singularity-free orientation representation

1. Introduction

The new generation of robots should have the intrinsic ability to share the operational environment with humans. Often physical interaction occurs, and this may happen at any part of the manipulator body. The contact can be both intentional (i.e., required for collaborative tasks) or unintentional (i.e., unexpected collisions). To guarantee a safe robot reaction to physical interaction, suitable control strategies must be adopted, which may require the measurement or the estimate of the the exchanged forces and moments, as well as the effective robot inertia, the relative velocity and the distance between the robot and the human [2].

One solution could be to cover the whole manipulator body with a sensitive skin [3] to obtain a direct measure of the exchanged force and moment as well as of the contact point. Nevertheless, this solution seems to be rather far to be applied at the moment. In case it is not possible to cover the arm with sensors, an alternative solution is to estimate the exchanged forces and moments on the basis of the available measures of joints position and/or torque, by using suitable observers [4] or neural interpolators [5]. This approach is adopted in [6] for collision detection and safe reaction.

For safety reasons, in order to keep limited the exchanged forces and moments, the manipulator is often requested to be compliant in response to physical interaction. From a mechanical point of view, such compliance can be passively achieved by using elastic decouplings between the actuators and the commanded links through fixed or variable joint stiffness [7]. On the other hand, active compliance relies on the control action, and impedance control is the widest adopted approach to actively control the robot compliance [8, 9, 10, 11]. If the external interaction is likely to occur only on some parts of the manipulator (i.e., the end-effector), a force/torque sensor helps in fully control the desired interaction with the environment via software. In case of redundant robots, a compliant behaviour can be imposed so as not to interfere with the main task [10, 12], an thus the so called null-space compliance or impedance is obtained. This is particularly useful in those situations where it is desirable to have the control of the interaction within the joint space. In such cases, the external forces affecting the main task must be suitably measured and/or estimated to allow an impedance behaviour as a secondary task without compromising the main one. Null-space impedance can be also achieved in multi-priority framework at acceleration level [12],

*Correspondig author

Email address: fabio.ruggiero@unina.it (Fabio Ruggiero)

or employing both a task error-based disturbance observer and a momentum-based observer [1]. A particular feature of the algorithm developed in [1] is that it allows to fully compensate the error in the task space caused by the physical interaction. Of course, this is possible only if the robot possesses a sufficient number of redundant degrees of freedom. In some applications, it is advisable to select a minimal number of task variables to be kept unaffected in the case of physical interaction. Moreover, the task variables are usually a subset of those representing the end-effector position and orientation. For example, if a robot waiter is carrying a trail with some food, when somebody pushes the arm, it is important to avoid the change of orientation of the trail, or, at least, any roll and pitch motions. Other approaches with redundant robots do not instead explicitly require the use of an active or passive compliance, but the manipulator's posture is optimized to minimize the impact/external wrench while carrying out the main task [13].

This work further develops what presented in [1], where the algorithm is presented with reference to generic task variables. In this paper, instead, the task variables are explicitly the position and orientation of the end effector. The orientation is considered in a non-minimal singularity free representation, *e.g.*, axis-angle, unit quaternion. Notice that using one of these two orientation representations, the theoretical framework within [1] fails since the closed-loop equations related to the angular part are not in a linear form. As in [1], the pursued goal is to control the robot manipulator in the Cartesian space while achieving an active compliant behaviour in the null-space. A dynamic term filtering both the effects of velocity and external forces is added to the controller to solve the task. A rigorous stability analysis is also provided. Notice that neither joint torque sensors nor force/torque sensors at the end-effector are required to accomplish the sought job.

The outline of the manuscript is as follows. Section 2 presents the mathematical background necessary to introduce the proposed control in Section 3. The stability proof of the closed-loop system is carried out in Section 4. Experiments confirming the provided theory are provided in Section 5. Section 6 finally concludes the manuscript.

2. Background

The equations of motion of a n joints robot arm can be written in the joint space according to the following compact matrix form [8]

$$\boldsymbol{B}(\boldsymbol{q})\ddot{\boldsymbol{q}} + \boldsymbol{C}(\boldsymbol{q},\dot{\boldsymbol{q}})\dot{\boldsymbol{q}} + \boldsymbol{g}(\boldsymbol{q}) = \boldsymbol{\tau} - \boldsymbol{\tau}_{ext}, \quad (1)$$

where $\boldsymbol{q} \in \mathbb{R}^n$, $\dot{\boldsymbol{q}} \in \mathbb{R}^n$ and $\ddot{\boldsymbol{q}} \in \mathbb{R}^n$ are the position, velocity and acceleration joint vectors, respectively; $\boldsymbol{B}(\boldsymbol{q}) \in \mathbb{R}^{n\times n}$ is the inertia matrix in the joint space; $\boldsymbol{C}(\boldsymbol{q},\dot{\boldsymbol{q}}) \in \mathbb{R}^{n\times n}$ is the matrix collecting Coriolis and centrifugal effects; $\boldsymbol{g}(\boldsymbol{q}) \in \mathbb{R}^n$ is the gravity vector term; $\boldsymbol{\tau} \in \mathbb{R}^n$ is the control torques vector; $\boldsymbol{\tau}_{ext} \in \mathbb{R}^n$ is the vector representing the external torques acting on the joints.

Notice that $\boldsymbol{\tau}_{ext}$ is a disturbance representing both joints torque due to the physical interaction with the environment and unmodelled effects. In this paper, it is assumed that the manipulator is equipped neither with torque sensors in the joints, nor with force/torque sensors. Therefore, it is not possible to measure $\boldsymbol{\tau}_{ext}$.

Considering a redundant manipulator ($n > 6$, in general), a joint space impedance control can be achieved in the null-space of the Cartesian task, or using a multi-priority redundancy resolution scheme [14]. Let Σ_i and Σ_e be the inertial and end-effector reference frames, respectively. Denote with $\boldsymbol{p}_e \in \mathbb{R}^3$ and $\boldsymbol{R}_e \in SO(3)$ the position and the orientation, respectively, of Σ_e in Σ_i. Consider the vector $\boldsymbol{\upsilon} = \begin{bmatrix}\dot{\boldsymbol{p}}_e^{\mathrm{T}} & \boldsymbol{\omega}_e^{\mathrm{T}}\end{bmatrix}^{\mathrm{T}} \in \mathbb{R}^6$, where $\boldsymbol{\omega}_e \in \mathbb{R}^3$ is the angular velocity of Σ_e with respect to Σ_i. The following relation between the joints velocity and the end-effector velocity holds

$$\boldsymbol{\upsilon} = \boldsymbol{J}(\boldsymbol{q})\dot{\boldsymbol{q}}, \quad (2)$$

where $\boldsymbol{J}(\boldsymbol{q}) \in \mathbb{R}^{6\times n}$ is the so-called geometric Jacobian of the robot arm [8]. A general inverse solution to (2) is given by $\dot{\boldsymbol{q}} = \boldsymbol{J}(\boldsymbol{q})^{\dagger}\boldsymbol{\upsilon} + \boldsymbol{N}(\boldsymbol{q})\dot{\boldsymbol{q}}_N$, where $\boldsymbol{J}(\boldsymbol{q})^{\dagger} \in \mathbb{R}^{n\times 6}$ is any generalized inverse of $\boldsymbol{J}(\boldsymbol{q})$, and $\boldsymbol{N} \in \mathbb{R}^{n\times n}$ is the matrix projecting the vector $\dot{\boldsymbol{q}}_N \in \mathbb{R}^n$ to the null-space of $\boldsymbol{J}(\boldsymbol{q})$. The vector $\dot{\boldsymbol{q}}_N$ represents internal redundancy motions of the manipulator joints that do not affect the end-effector velocity $\boldsymbol{\upsilon}$. It is assumed that the robot does not pass close to singular joint configurations, i.e. $\boldsymbol{J}(\boldsymbol{q})$ is full rank.

In order to better characterise the internal motions of a redundant manipulator, one solution is to use the so-called *joint space decomposition method* [10]. In this case the Cartesian coordinates

are augmented by adding $r = n - 6$ auxiliary variables $\boldsymbol{\lambda} \in \mathbb{R}^r$ to the end-effector velocity $\boldsymbol{v}$. These auxiliary variables are defined as

$$\dot{\boldsymbol{q}} = \boldsymbol{N}\dot{\boldsymbol{q}}_N = \boldsymbol{Z}(\boldsymbol{q})\boldsymbol{\lambda}, \tag{3}$$

where $\boldsymbol{Z}(\boldsymbol{q}) \in \mathbb{R}^{n\times r}$ is such that $\boldsymbol{J}(\boldsymbol{q})\boldsymbol{Z}(\boldsymbol{q}) = \boldsymbol{O}_{6\times r}$, where $\boldsymbol{O}_{a\times b} \in \mathbb{R}^{a\times b}$ is a zero matrix of proper dimensions. Therefore $\boldsymbol{Z}(\boldsymbol{q})$ is a matrix spanning the null-space of $\boldsymbol{J}(\boldsymbol{q})$. Having in mind (3), a convenient choice for $\boldsymbol{\lambda}$ is given by the left inertia-weighted generalized inverse of $\boldsymbol{Z}(\boldsymbol{q})$ [15], such that $\boldsymbol{\lambda} = \boldsymbol{Z}(\boldsymbol{q})^{\#}\dot{\boldsymbol{q}}$, with $\boldsymbol{Z}(\boldsymbol{q})^{\#} = \left(\boldsymbol{Z}(\boldsymbol{q})^{\mathrm{T}}\boldsymbol{B}(\boldsymbol{q})\boldsymbol{Z}(\boldsymbol{q})\right)^{-1}\boldsymbol{Z}(\boldsymbol{q})^{\mathrm{T}}\boldsymbol{B}(\boldsymbol{q})$. By this choice, it is possible to extend (2) through the following form

$$\boldsymbol{\xi} = \begin{bmatrix}\boldsymbol{v}\\ \boldsymbol{\lambda}\end{bmatrix} = \boldsymbol{J}_E(\boldsymbol{q})\dot{\boldsymbol{q}} = \begin{bmatrix}\boldsymbol{J}(\boldsymbol{q})\\ \boldsymbol{Z}(\boldsymbol{q})^{\#}\end{bmatrix}\dot{\boldsymbol{q}}, \tag{4}$$

where

$$\boldsymbol{J}_E(\boldsymbol{q})^{-1} = \begin{bmatrix}\boldsymbol{J}(\boldsymbol{q})^{\#} & \boldsymbol{Z}(\boldsymbol{q})\end{bmatrix}, \tag{5}$$

is non-singular for full rank matrix $\boldsymbol{J}(\boldsymbol{q})$, and $\boldsymbol{J}(\boldsymbol{q})^{\#} = \boldsymbol{B}(\boldsymbol{q})^{-1}\boldsymbol{J}(\boldsymbol{q})^{\mathrm{T}}\left(\boldsymbol{J}(\boldsymbol{q})\boldsymbol{B}(\boldsymbol{q})^{-1}\boldsymbol{J}(\boldsymbol{q})^{\mathrm{T}}\right)^{-1}$ is the so-called dynamically consistent generalized inverse Jacobian [16], which plays a key role in null-space dynamics [10]. Therefore, the following decompositions for the joints velocity and acceleration hold

$$\dot{\boldsymbol{q}} = \boldsymbol{J}(\boldsymbol{q})^{\#}\boldsymbol{v} + \boldsymbol{Z}(\boldsymbol{q})\boldsymbol{\lambda}, \tag{6}$$

$$\ddot{\boldsymbol{q}} = \boldsymbol{J}_E^{-1}(\boldsymbol{q})\dot{\boldsymbol{\xi}} + \dot{\boldsymbol{J}}_E^{-1}(\boldsymbol{q})\boldsymbol{\xi}. \tag{7}$$

The complete dynamic model in both the task and the null-space can be found in [10]: the related derivation is here avoided.

The control objective is to satisfy a task in the Cartesian space while achieving a compliant behaviour for the manipulator, without affecting the main task. This will be also possible thanks to the aforementioned choice of considering geometric consistent generalized inverse matrices whose metric is induced by the inertia matrix. The following controller is then consider for the dynamic system (1)

$$\boldsymbol{\tau} = \boldsymbol{B}(\boldsymbol{q})\boldsymbol{u}_q + \boldsymbol{C}(\boldsymbol{q},\dot{\boldsymbol{q}})\dot{\boldsymbol{q}} + \boldsymbol{g}(\boldsymbol{q}), \tag{8}$$

where $\boldsymbol{u}_q \in \mathbb{R}^n$ is a new virtual control input having the dimension of joints acceleration. The closed-loop dynamics assume the following form

$$\ddot{\boldsymbol{q}} = \boldsymbol{u}_q - \boldsymbol{B}(\boldsymbol{q})^{-1}\boldsymbol{\tau}_{ext}. \tag{9}$$

Having in mind (7) and (9), the following command acceleration can be considered [1]

$$\boldsymbol{u}_q = \boldsymbol{J}(\boldsymbol{q})^{\#}\left(\boldsymbol{u}_v - \dot{\boldsymbol{J}}(\boldsymbol{q})\dot{\boldsymbol{q}}\right) + \boldsymbol{Z}(\boldsymbol{q})\left(\boldsymbol{u}_\lambda - \dot{\boldsymbol{Z}}(\boldsymbol{q})^{\#}\dot{\boldsymbol{q}}\right), \tag{10}$$

where $\boldsymbol{u}_v \in \mathbb{R}^6$ and $\boldsymbol{u}_\lambda \in \mathbb{R}^r$ are new virtual control inputs having the dimension of Cartesian and null-space accelerations, respectively. Folding (10) in (9), and in turn in (7), it is then possible to project the closed-loop dynamics in the Cartesian space and in the null-space by multiplying both sides of the resulting equation by $\boldsymbol{J}(\boldsymbol{q})$ and $\boldsymbol{Z}(\boldsymbol{q})^{\#}$, respectively, yielding

$$\dot{\boldsymbol{v}} = \boldsymbol{u}_v - \boldsymbol{J}(\boldsymbol{q})\boldsymbol{B}(\boldsymbol{q})^{-1}\boldsymbol{\tau}_{ext}, \tag{11}$$

$$\dot{\boldsymbol{\lambda}} = \boldsymbol{u}_\lambda - \boldsymbol{Z}(\boldsymbol{q})^{\#}\boldsymbol{B}(\boldsymbol{q})^{-1}\boldsymbol{\tau}_{ext}. \tag{12}$$

In the next section, the design of $\boldsymbol{u}_v$ and $\boldsymbol{u}_\lambda$ is addressed.

3. Controllers

3.1. Controller for the main task

The main task for the robot consists in a desired trajectory in the Cartesian space, expressed in terms of position and orientation of the end-effector. For the orientation, a general non-minimum singularity free representation is adopted. From (11) it is possible to notice how the external torques applied to the manipulators may interfere with the main task. An effective solution to this problem is that of compensating the effects of $\boldsymbol{\tau}_{ext}$ in the control law by using a suitable estimate of this and compensating for its effects.

The desired trajectory for Σ_e is specified in terms of the desired position $\boldsymbol{p}_d \in \mathbb{R}^3$, orientation $\boldsymbol{R}_d \in SO(3)$, linear velocity $\dot{\boldsymbol{p}}_d \in \mathbb{R}^3$, angular velocity $\boldsymbol{\omega}_d \in \mathbb{R}^3$, linear acceleration $\ddot{\boldsymbol{p}}_d \in \mathbb{R}^3$ and angular acceleration $\dot{\boldsymbol{\omega}}_d \in \mathbb{R}^3$, all with respect to Σ_i. Having at disposition the current value of orientation $\boldsymbol{R}_e$, it is possible to define the deviation matrix $\widetilde{\boldsymbol{R}} = \boldsymbol{R}_d^{\mathrm{T}}\boldsymbol{R}_e \in SO(3)$.

A non-minimal representation for the deviation rotation matrix $\widetilde{\boldsymbol{R}}$ can be obtained by resorting to 4 parameters $\boldsymbol{\alpha} \in \mathbb{R}^4$ [8, 17]. Therefore, from $\widetilde{\boldsymbol{R}}$ it is possible to express the orientation error also as $\widetilde{\boldsymbol{o}} = \boldsymbol{f}_o(\boldsymbol{\alpha}) \in \mathbb{R}^3$, with $\boldsymbol{f}_o$ a generic vector function of $\boldsymbol{\alpha}$ and the property that $\dot{\widetilde{\boldsymbol{o}}} = \boldsymbol{L}(\boldsymbol{\alpha})\widetilde{\boldsymbol{\omega}}$, where $\boldsymbol{L}(\boldsymbol{\alpha}) \in \mathbb{R}^{3\times 3}$ is a nonsingular matrix and $\widetilde{\boldsymbol{\omega}} = \boldsymbol{\omega}_e - \boldsymbol{\omega}_d \in \mathbb{R}^3$ is the angular velocity error. Particular expressions regarding angle/axis

and unit quaternion representations are given in the Appendix.

In order to impose the main task, the controller is then designed as follows

$$\boldsymbol{u}_{\upsilon} = \dot{\boldsymbol{\upsilon}}_d + \boldsymbol{D}_{\upsilon}\boldsymbol{e}_{\upsilon} + \boldsymbol{K}_{\upsilon}\boldsymbol{e}_t - \boldsymbol{J}(\boldsymbol{q})\boldsymbol{B}(\boldsymbol{q})^{-1}\boldsymbol{\gamma}, \quad (13a)$$

$$\dot{\boldsymbol{\gamma}} = -\boldsymbol{K}_I(\boldsymbol{\gamma} + \boldsymbol{\tau}_{ext}) + \boldsymbol{K}_{\gamma}^{-1}\boldsymbol{B}(\boldsymbol{q})^{-1}\boldsymbol{J}(\boldsymbol{q})^{\mathrm{T}}\boldsymbol{\upsilon}, \quad (13b)$$

where $\dot{\boldsymbol{\upsilon}}_d = \begin{bmatrix}\ddot{\boldsymbol{p}}_d^{\mathrm{T}} & \dot{\boldsymbol{\omega}}_d^{\mathrm{T}}\end{bmatrix}^{\mathrm{T}} \in \mathbb{R}^6$, $\boldsymbol{e}_{\upsilon} = \begin{bmatrix}\dot{\widetilde{\boldsymbol{p}}}^{\mathrm{T}} & \widetilde{\boldsymbol{\omega}}^{\mathrm{T}}\end{bmatrix}^{\mathrm{T}} \in \mathbb{R}^6$, $\boldsymbol{e}_t = \begin{bmatrix}\widetilde{\boldsymbol{p}}^{\mathrm{T}} & \widetilde{\boldsymbol{o}}^{\mathrm{T}}\end{bmatrix}^{\mathrm{T}} \in \mathbb{R}^6$, $\dot{\widetilde{\boldsymbol{p}}} = \dot{\boldsymbol{p}}_d - \dot{\boldsymbol{p}}_e \in \mathbb{R}^3$, $\widetilde{\boldsymbol{p}} = \boldsymbol{p}_d - \boldsymbol{p}_e \in \mathbb{R}^3$, $\boldsymbol{\gamma} \in \mathbb{R}^n$, $\boldsymbol{K}_{\upsilon} = \mathrm{diag}(\boldsymbol{K}_p, \boldsymbol{K}_o) \in \mathbb{R}^{6\times 6}$ with $\boldsymbol{K}_p \in \mathbb{R}^{3\times 3}$ a positive definite diagonal gain matrix and $\boldsymbol{K}_o \in \mathbb{R}^{3\times 3}$ an invertible matrix. Finally, $\boldsymbol{D}_{\upsilon} \in \mathbb{R}^{6\times 6}$, $\boldsymbol{K}_I \in \mathbb{R}^{n\times n}$, and $\boldsymbol{K}_{\gamma} \in \mathbb{R}^{n\times n}$ are positive definite diagonal gain matrices.

In order to compute (13b), notice how the measure of the external forces $\boldsymbol{\tau}_{ext}$ is in principle required. The manipulator dynamic model (1) might be inverted so as to express $\boldsymbol{\tau}_{ext}$ as a function of the control input $\boldsymbol{\tau}$ and of other terms dependent on the joint positions, velocity and accelerations. However, it is not difficult to show that equation (13b) has a closed-form integral which can be directly folded in (13a)

$$\begin{aligned}\boldsymbol{\gamma}(t) = \boldsymbol{K}_I \Bigg(& \boldsymbol{B}(\boldsymbol{q})\dot{\boldsymbol{q}} \\ & - \int_0^t \left(\boldsymbol{\tau} + \boldsymbol{C}(\boldsymbol{q},\dot{\boldsymbol{q}})^{\mathrm{T}}\dot{\boldsymbol{q}} - \boldsymbol{g}(\boldsymbol{q}) + \boldsymbol{\gamma}(\sigma)\right)\mathrm{d}\sigma \Bigg) \\ & + \boldsymbol{K}_{\gamma}^{-1}\int_0^t \boldsymbol{B}(\boldsymbol{q})^{-1}\boldsymbol{J}(\boldsymbol{q})^{\mathrm{T}}\boldsymbol{\upsilon}\mathrm{d}\sigma,\end{aligned} \quad (14)$$

where the measure neither of the joints acceleration nor of the external forces is required. Notice that the first term of (14) is equal to the momentum-based observer of the external forces introduced in [6]. It is thus possible to affirm that the dynamic term $\boldsymbol{\gamma}$ tends to $-\boldsymbol{\tau}_{ext}$ at steady-state, provided that $\boldsymbol{K}_I$ is large enough [6].

Folding (13a) in (11), the corresponding Cartesian space closed-loop equation is

$$\dot{\boldsymbol{e}}_{\upsilon} + \boldsymbol{D}_{\upsilon}\boldsymbol{e}_{\upsilon} + \boldsymbol{K}_{\upsilon}\boldsymbol{e}_t = \boldsymbol{J}(\boldsymbol{q})\boldsymbol{B}(\boldsymbol{q})^{-1}\boldsymbol{e}_{\gamma}, \quad (15)$$

with $\boldsymbol{e}_{\gamma} = \boldsymbol{\gamma} + \boldsymbol{\tau}_{ext} \in \mathbb{R}^n$. Since at steady-state $\boldsymbol{\gamma} \to -\boldsymbol{\tau}_{ext}$, then $\boldsymbol{e}_{\gamma} \to \boldsymbol{0}_n$, with $\boldsymbol{0}_a \in \mathbb{R}^a$ a zero vector. In this case, equation (15) is homogeneous for the position part, but not for the orientation one. Nevertheless, considering either angle/axis or unit quaternion representations, it is possible to show that the errors goes asymptotically to zero [17]. During motion this is not true. Asymptotically stability is anyway preserved in case of constant external forces, i.e. $\dot{\boldsymbol{\tau}}_{ext} = \boldsymbol{0}_n$, as derived in Section 4.

3.2. Null-space impedance controller

In general, the null-space velocity vector $\boldsymbol{\lambda}$ is not integrable [18] and, thus, a null-space position error cannot be defined. The null-space commanded acceleration is then taken as in [1, 19]

$$\begin{aligned}\boldsymbol{u}_{\lambda} = \dot{\boldsymbol{\lambda}}_d + \boldsymbol{\Lambda}_{\lambda}(\boldsymbol{q})^{-1}\big(& (\boldsymbol{\mu}_{\lambda}(\boldsymbol{q},\dot{\boldsymbol{q}}) + \boldsymbol{D}_{\lambda})\,\boldsymbol{e}_{\lambda} \\ & + \boldsymbol{Z}(\boldsymbol{q})^{\mathrm{T}}\left(\boldsymbol{K}_q\boldsymbol{e}_q + \boldsymbol{D}_q\dot{\boldsymbol{e}}_q\right)\big),\end{aligned} \quad (16)$$

with $\boldsymbol{\Lambda}_{\lambda}(\boldsymbol{q}) = \boldsymbol{Z}(\boldsymbol{q})^{\mathrm{T}}\boldsymbol{B}(\boldsymbol{q})\boldsymbol{Z}(\boldsymbol{q}) \in \mathbb{R}^{r\times r}$, $\boldsymbol{\mu}_{\lambda}(\boldsymbol{q},\dot{\boldsymbol{q}}) = \left(\boldsymbol{Z}(\boldsymbol{q})^{\mathrm{T}}\boldsymbol{C}(\boldsymbol{q},\dot{\boldsymbol{q}}) - \boldsymbol{\Lambda}_{\lambda}(\boldsymbol{q})\dot{\boldsymbol{Z}}(\boldsymbol{q})^{\#}\right)\boldsymbol{Z}(\boldsymbol{q}) \in \mathbb{R}^{r\times r}$, $\boldsymbol{e}_{\lambda} = \boldsymbol{\lambda}_d - \boldsymbol{\lambda} \in \mathbb{R}^r$, $\boldsymbol{e}_q = \boldsymbol{q}_d - \boldsymbol{q} \in \mathbb{R}^n$. The quantities $\boldsymbol{\lambda}_d \in \mathbb{R}^r$ and $\dot{\boldsymbol{\lambda}}_d \in \mathbb{R}^r$ are the null-space desired velocity and acceleration vectors, respectively, while $\boldsymbol{D}_{\lambda} \in \mathbb{R}^{r\times r}$, $\boldsymbol{K}_q \in \mathbb{R}^{n\times n}$, and $\boldsymbol{D}_q \in \mathbb{R}^{n\times n}$ are definite positive gain matrices, and $\boldsymbol{q}_d \in \mathbb{R}^n$ is the constant desired value of the joint positions. Notice that the term $\boldsymbol{D}_q\dot{\boldsymbol{e}}_q$ is not present in [1]: here such derivative term is added to improve control performance. Folding (16) in (12), the null-space closed-loop equation is obtained

$$\begin{aligned}&\boldsymbol{\Lambda}_{\lambda}(\boldsymbol{q})\dot{\boldsymbol{e}}_{\lambda} + (\boldsymbol{\mu}_{\lambda}(\boldsymbol{q},\dot{\boldsymbol{q}}) + \boldsymbol{D}_{\lambda})\,\boldsymbol{e}_{\lambda} \\ &\quad + \boldsymbol{Z}(\boldsymbol{q})^{\mathrm{T}}\left(\boldsymbol{K}_q\boldsymbol{e}_q + \boldsymbol{D}_q\dot{\boldsymbol{e}}_q\right) = \boldsymbol{Z}(\boldsymbol{q})^{\mathrm{T}}\boldsymbol{\tau}_{ext}.\end{aligned} \quad (17)$$

Equation (17) can be seen as an impedance equation defined in the null-space. The null-space inertia matrix $\boldsymbol{\Lambda}_{\lambda}(\boldsymbol{q})$ and the null-space Coriolis matrix $\boldsymbol{\mu}_{\lambda}(\boldsymbol{q},\dot{\boldsymbol{q}})$ cannot be modified, while matrices $\boldsymbol{D}_{\lambda}$, $\boldsymbol{K}_q$ and $\boldsymbol{D}_q$ can be tuned to specify the null-space behiaviour. The vector on the right side of the equation is the null-space projection of the external torques. Notice that $\boldsymbol{\Lambda}_{\lambda}(\boldsymbol{q})$ is positive definite and $\dot{\boldsymbol{\Lambda}}_{\lambda}(\boldsymbol{q}) - 2\boldsymbol{\mu}_{\lambda}(\boldsymbol{q},\dot{\boldsymbol{q}})$ is skew-symmetric [1].

4. Stability proof

The resulting block scheme of the proposed controller is depicted in Figure 1. Given the designed control inputs (13a), (14) and (16) the closed loop system equations are given by (15) and (17). This section is devoted to show that the system state $\boldsymbol{x} = (\boldsymbol{e}_q, \boldsymbol{e}_t, \boldsymbol{e}_{\upsilon}, \boldsymbol{e}_{\gamma}, \boldsymbol{e}_{\lambda}) \in \mathbb{R}^m$, with $m = 2n+r+12$, goes asymptotically to zero. The stability proof is based on the concept of conditional stability [19]. The following theorem is thus firstly introduced.

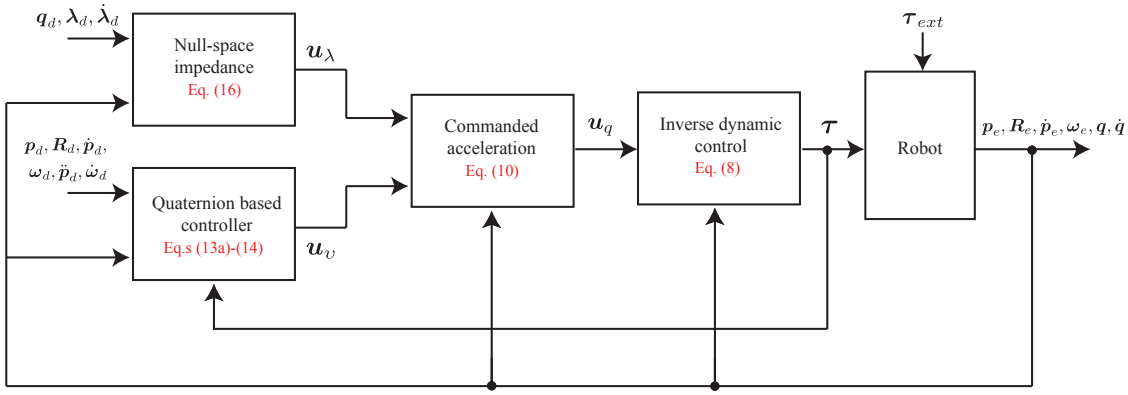

Figure 1: Block scheme of the proposed control architecture. In red, the related corresponding equations in the paper. The full robot state enters in each block only for readability reasons.

Theorem 1. *Consider a system $\dot{\boldsymbol{x}} = \boldsymbol{f}(\boldsymbol{x})$, with $\boldsymbol{f}(\boldsymbol{x}) \in \mathbb{R}^m$, with $\boldsymbol{x} = \boldsymbol{0}_m$ an equilibrium point. If in a neighbourhood Ω of this equilibrium point there exists a scalar continuous function $V \in \mathcal{C}^1$ such that*

1. *$V(\boldsymbol{x}) \geq 0$ for all $\boldsymbol{x} \in \Omega$ and $V(\boldsymbol{0}_m) = 0$;*
2. *$\dot{V}(\boldsymbol{x}) \leq 0$ for all $\boldsymbol{x} \in \Omega$;*
3. *on the largest positive invariant set $\mathcal{L} \subseteq \mathcal{Y} = \{\boldsymbol{x} \in \Omega : \dot{V}(\boldsymbol{x}) = 0\}$, the system is asymptotically stable;*

then the equilibrium point is asymptotically stable for the system.

Proof. See [20]. □

It is then possible to introduce and prove the following proposition.

Proposition 1. *Given a redundant robot arm whose dynamic model is given by (1), the control law represented by equations (8), (13a), (14) and (16) is able to guarantee regulation of a desired task in the Cartesian space, while providing a compliant behaviour in the null-space. Namely, provided that $\boldsymbol{K}_v$ is a block-diagonal invertible matrix, $\boldsymbol{D}_v, \boldsymbol{K}_I, \boldsymbol{K}_\gamma, \boldsymbol{K}_q, \boldsymbol{D}_q, \boldsymbol{D}_\lambda$ are diagonal and positive definite matrices, and assumed that $\dot{\boldsymbol{\tau}}_{ext} = \dot{\boldsymbol{q}}_d = \boldsymbol{0}_n$, $\dot{\boldsymbol{p}}_d = \boldsymbol{\omega}_d = \boldsymbol{0}_3$ and $\boldsymbol{\lambda}_d = \boldsymbol{0}_r$, then*

1. *the state $\boldsymbol{x} = (\boldsymbol{e}_q, \boldsymbol{e}_t, \boldsymbol{e}_v, \boldsymbol{e}_\gamma, \boldsymbol{e}_\lambda)$ goes asymptotically to zero if $\boldsymbol{\tau}_{ext} = \boldsymbol{0}_n$, and $\boldsymbol{q}_d$ is chosen such that the manipulator end-effector is in the pose $(\boldsymbol{p}_d, \boldsymbol{R}_d)$;*
2. *the state $\boldsymbol{x} = (\boldsymbol{q} \to \boldsymbol{q}^\star, \boldsymbol{e}_t \to \boldsymbol{0}_6, \boldsymbol{e}_v \to \boldsymbol{0}_6, \boldsymbol{e}_\gamma \to \boldsymbol{0}_n, \boldsymbol{e}_\lambda \to \boldsymbol{0}_r)$ if $\boldsymbol{\tau}_{ext} \neq \boldsymbol{0}_n$ and/or $\boldsymbol{q}_d$ is chosen such that the manipulator end-effector is not in the pose $(\boldsymbol{p}_d, \boldsymbol{R}_d)$. The term $\boldsymbol{q}^\star \in \mathbb{R}^n$ belongs to the set of solutions which locally minimizes the quadratic function $\|\boldsymbol{K}_q \boldsymbol{e}_q + \boldsymbol{D}_q \dot{\boldsymbol{e}}_q - \boldsymbol{\tau}_{ext}\|^2$ subject to the condition that the manipulator end-effector is located at $(\boldsymbol{p}_d, \boldsymbol{R}_d)$.*

Proof. This proof is based on Theorem 1. Consider a neighbourhood Ω of the origin $\boldsymbol{x} = \boldsymbol{0}_m$. Define the following scalar function

$$V(\boldsymbol{e}_v, \boldsymbol{e}_t, \boldsymbol{e}_\gamma) = \frac{1}{2}\boldsymbol{e}_v^{\mathrm{T}}\boldsymbol{e}_v + \frac{1}{2}\boldsymbol{e}_t^{\mathrm{T}}\boldsymbol{K}_V\boldsymbol{e}_t + \frac{1}{2}\boldsymbol{e}_\gamma^{\mathrm{T}}\boldsymbol{K}_\gamma\boldsymbol{e}_\gamma + f_V(\boldsymbol{\alpha}), \tag{18}$$

with $\boldsymbol{K}_V = \mathrm{diag}(\boldsymbol{K}_p, \boldsymbol{K}_{V,2}) \in \mathbb{R}^{6\times 6}$, where $\boldsymbol{K}_{V,2} \in \mathbb{R}^{3\times 3}$ is a positive definite diagonal matrix, and $f_V(\boldsymbol{\alpha}) \in \mathbb{R} \geq 0$. Such a function must have the following properties

$$f_V(\boldsymbol{\alpha}) = 0, \quad \text{if} \quad \tilde{\boldsymbol{o}} = \boldsymbol{0}_3, \tag{19a}$$

$$\dot{f}_V(\boldsymbol{\alpha}) = \tilde{\boldsymbol{\omega}}^{\mathrm{T}} \left(\boldsymbol{K}_o - \boldsymbol{L}(\boldsymbol{\alpha})^{\mathrm{T}}\boldsymbol{K}_{V,2}\right)\tilde{\boldsymbol{o}}. \tag{19b}$$

Notice that $V(\boldsymbol{e}_v, \boldsymbol{e}_t, \boldsymbol{e}_\gamma)$ is positive semi-definite in Ω and $V(\boldsymbol{0}_m) = 0$, satisfying the first point of Theorem 1. The detailed expressions of f_V, $\boldsymbol{K}_o$ and $\boldsymbol{K}_{V,2}$ for the angle/axis and unit quaternion representations are given in the Appendix.

Taking into account the expression for $\dot{\tilde{\boldsymbol{o}}}$, the time derivative of $\boldsymbol{e}_t$ is

$$\dot{\boldsymbol{e}}_t = \begin{bmatrix} \boldsymbol{I}_3 & \boldsymbol{O}_3 \\ \boldsymbol{O}_3 & \boldsymbol{L}(\boldsymbol{\alpha}) \end{bmatrix} \boldsymbol{e}_v, \tag{20}$$

where $\boldsymbol{I}_a \in \mathbb{R}^{a\times a}$ is the identity matrix. On the other hand, since for assumption $\dot{\boldsymbol{\tau}}_{ext} = \boldsymbol{0}_n$, then

$$\dot{\boldsymbol{e}}_\gamma = \dot{\boldsymbol{\gamma}}, \tag{21}$$

whose complete expression is given in (13b). Therefore, having in mind (15), (19b), (20) and (21), deriving (18) with respect to time yields

$$\dot{V} = -\boldsymbol{e}_{\upsilon}^{\mathrm{T}} \boldsymbol{D}_{\upsilon} \boldsymbol{e}_{\upsilon} - \boldsymbol{e}_{\gamma}^{\mathrm{T}} \boldsymbol{K}_{\gamma} \boldsymbol{K}_{I} \boldsymbol{e}_{\gamma}. \tag{22}$$

Notice that (22) is negative semi-definite in Ω, satisfying the second point of Theorem 1.

Consider the set $\mathcal{Y} = \{\boldsymbol{x} \in \Omega : \boldsymbol{e}_q, \boldsymbol{e}_t, \boldsymbol{e}_{\upsilon} = \boldsymbol{0}_6, \boldsymbol{e}_{\gamma} = \boldsymbol{0}_r, \boldsymbol{e}_{\lambda}\}$. With the given assumptions, notice that in this set $\boldsymbol{\upsilon} = \boldsymbol{0}_6$. Point 3 of Theorem 1 is now addressed. Define the following candidate Lyapunov function

$$V_{\mathcal{Y}} = \frac{1}{2} \boldsymbol{e}_{\lambda}^{\mathrm{T}} \boldsymbol{\Lambda}_{\lambda}(\boldsymbol{q}) \boldsymbol{e}_{\lambda} + \frac{1}{2} \boldsymbol{e}_{t}^{\mathrm{T}} \boldsymbol{e}_{t} + \frac{1}{2} \boldsymbol{e}_{q}^{\mathrm{T}} \boldsymbol{K}_{q} \boldsymbol{e}_{q}, \tag{23}$$

which it positive definite on $\mathcal{Y}$. Taking into account (6), (17), (20), and considering that $\dot{\boldsymbol{e}}_q = -\dot{\boldsymbol{q}}$ and $\boldsymbol{e}_{\lambda} = -\boldsymbol{\lambda}$, the time derivative of (23) within $\mathcal{Y}$ is

$$\begin{aligned} \dot{V}_{\mathcal{Y}} = &-\boldsymbol{\lambda}^{\mathrm{T}} \left(\boldsymbol{D}_{\lambda} + \boldsymbol{Z}(\boldsymbol{q})^{\mathrm{T}} \boldsymbol{D}_{q} \boldsymbol{Z}(\boldsymbol{q}) \right) \boldsymbol{\lambda} \\ &- \boldsymbol{\lambda}^{\mathrm{T}} \boldsymbol{Z}(\boldsymbol{q})^{\mathrm{T}} \boldsymbol{\tau}_{ext}. \end{aligned} \tag{24}$$

Taking into account (15), it is possible to notice that the equality $\boldsymbol{e}_t = \boldsymbol{0}_6$ holds within $\mathcal{Y}$. This implies both $\widetilde{\boldsymbol{p}} = \boldsymbol{0}_3$ and $\widetilde{\boldsymbol{o}} = \boldsymbol{0}_3$.

Consider the first point of Proposition 1. Since $\boldsymbol{\tau}_{ext} = \boldsymbol{0}_n$, then $\dot{V}_{\mathcal{Y}} = -\boldsymbol{\lambda}^{\mathrm{T}} \left(\boldsymbol{D}_{\lambda} + \boldsymbol{Z}(\boldsymbol{q})^{\mathrm{T}} \boldsymbol{D}_{q} \boldsymbol{Z}(\boldsymbol{q}) \right) \boldsymbol{\lambda} \leq -\boldsymbol{\lambda}^{\mathrm{T}} \boldsymbol{D}_{\lambda} \boldsymbol{\lambda}$, which is negative semi-definite in $\mathcal{Y}$. Therefore, $\boldsymbol{e}_{\lambda} \to \boldsymbol{0}_r$. Invoking the La Salle's invariance principle and having in mind (17), it is straightforward to prove that $\boldsymbol{e}_q \to \boldsymbol{0}_n$ [1]. Hence, for the above considerations, the system is asymptotically stable on the largest invariant set $\mathcal{L} \subseteq \mathcal{Y}$. This satisfies the third and last point of Theorem 1, and thus proves the first point of Proposition 1.

Consider the second point of Proposition 1. When an external torque $\boldsymbol{\tau}_{ext}$ is applied, and/or if the desired joints configuration $\boldsymbol{q}_d$ is not chosen such that the end-effector is located at the desired configuration $(\boldsymbol{p}_d, \boldsymbol{R}_d)$ with respect to Σ_i, the asymptotically stability of the system is still preserved but the system reaches a different equilibrium $\boldsymbol{x} = (\boldsymbol{q} \to \boldsymbol{q}^{\star}, \boldsymbol{e}_t \to \boldsymbol{0}_6, \boldsymbol{e}_{\upsilon} \to \boldsymbol{0}_6, \boldsymbol{e}_{\gamma} \to \boldsymbol{0}_n, \boldsymbol{e}_{\lambda} \to \boldsymbol{0}_r)$ as shown in [1]. This because the manipulator reaches a joints configuration $\boldsymbol{q}^{\star}$ which is compatible with the main task $(\boldsymbol{p}_d, \boldsymbol{R}_d)$ and minimizing the elastic potential energy $\|\boldsymbol{K}_q \boldsymbol{e}_q + \boldsymbol{D}_q \dot{\boldsymbol{e}}_q - \boldsymbol{\tau}_{ext}\|^2$. The solution of this minimization is $\boldsymbol{Z}(\boldsymbol{q})^{\mathrm{T}} \left(\boldsymbol{K}_q \boldsymbol{e}_q + \boldsymbol{D}_q \dot{\boldsymbol{e}}_q - \boldsymbol{\tau}_{ext} \right) = \boldsymbol{0}_r$. As a consequence, $\dot{V}_{\mathcal{Y}}$ is again less or equal to $-\boldsymbol{\lambda}^{\mathrm{T}} \boldsymbol{D}_{\lambda} \boldsymbol{\lambda}$, and thus $\boldsymbol{e}_{\lambda}$ tends to zero. Having also in mind the above considerations, this proves the second point of Proposition 1. □

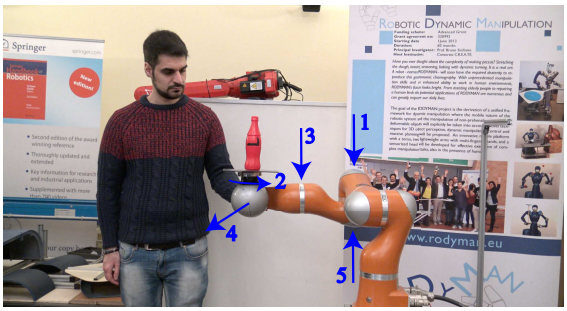

Figure 2: The KUKA LWR4 employed for the experiments in the initial, and desired, configuration for the joints, and with the desired orientation for the end-effector. The blue arrows represents the contacts with the operator during tasks. The label indicates the sequence of its contact.

5. Experiments

The performances of the proposed approach are experimentally verified on a KUKA LWR4. This robot arm has $n = 7$ joints, meaning that it is intrinsically redundant for any task fully defined in the Cartesian space. The control algorithm is written in C++ and executed on a remote PC with an UBUNTU OS. This remote PC is connected to a KUKA robot controller through UDP socket. The sampling rate is 2 ms. The data are exchanged through the FRI (Fast Research Interface) library [21].

In all of the performed experiments, an operator pushed the robot in different parts of its body. The main task of the controller is to keep fixed the initial orientation of the robot, while achieving null-space compliance. Therefore, the auxiliary variables $\boldsymbol{\lambda}$ have dimension $r = 4$. The null-space goal is to keep the initial position, denoted as $\boldsymbol{q}_d$. Without loss of generality, only the unit quaternion representation has been employed within the experiments. The desired velocities and accelerations in both spaces are zero. The initial configuration of the arm is depicted in Figure 2. In such a figure, the blue arrows indicate the performed contacts, while the labels indicate the sequence of each contact. The total time of the experiments is about 30 s. Having in mind that the above defined goals, the gains have been experimentally tuned to the

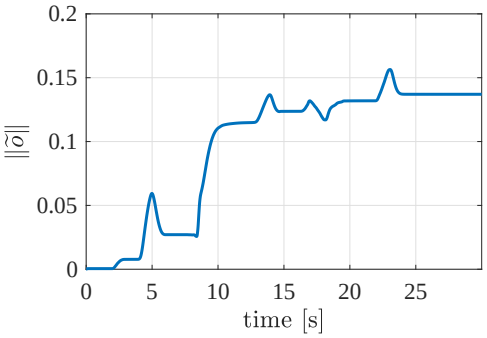

Figure 3: Time history of $\|\widetilde{\boldsymbol{o}}\|$ for the first case study.

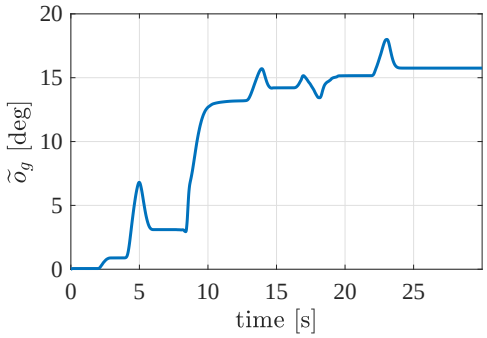

Figure 4: Time history of $\widetilde{o}_g$ for the first case study.

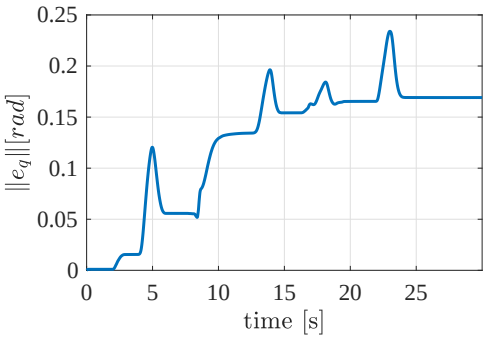

Figure 5: Time history of $\|\boldsymbol{e}_q\|$ for the first case study.

following values: $\boldsymbol{K}_p = \boldsymbol{O}_3$, $\boldsymbol{K}_o = 400\boldsymbol{I}_3$, $\boldsymbol{D}_v = \text{blockdiag}\{\boldsymbol{O}_3, 250\boldsymbol{I}_3\}$, $\boldsymbol{K}_I = 100\boldsymbol{I}_7$, $\boldsymbol{K}_\gamma = 100\boldsymbol{I}_7$, $\boldsymbol{K}_q = 30\boldsymbol{I}_7$, $\boldsymbol{D}_q = 5\boldsymbol{I}_7$, $\boldsymbol{D}_\lambda = 2\boldsymbol{I}_5$. As highlighted in [1], a particular care has to be put in the computation of $\boldsymbol{Z}(\boldsymbol{q})$, where numerical calculation may cause discontinuity in the solution. Mathematica software has been employed in this case to symbolically compute the matrix.

Two case studies are considered in the following, exploiting the idea of carrying a given object, *i.e.*, a bottle, on a tray (see Fig. 2). Namely, in the former case study, the $\boldsymbol{\gamma}$ term in (13a) is not taken into account, that is both $\boldsymbol{K}_I$ and $\boldsymbol{K}_\gamma^{-1}$ are set to zero in (14). The latter case study, instead, considers the controller as a whole. Other case studies are considered within the multimedia attachment: i) In order to test the performance of the sole pose controller, the null-space stiffness gain $\boldsymbol{K}_\lambda$ is set to zero. In this way, the behaviour is very similar to a zero-force control. ii) The performance of the proposed controller in case of impulsive external forces is shown through the robustness of the robot to unintentional collisions. This is also useful to bolster the effectiveness of the approach in human-robot interaction applications, like the case of a robotic waiter carrying objects on a tray in a crowded environment.

5.1. Case Study 1

In this case study, the matrix gains $\boldsymbol{K}_I$ and $\boldsymbol{K}_\gamma^{-1}$ are set to zero. This means that $\boldsymbol{\gamma}$ within (13a) is zero. Time histories of the performed experiments are depicted from Fig. 3 to Fig. 6.

The deviation of the orientation of Σ_e from the initial configuration, i.e. the time history of $\|\widetilde{\boldsymbol{o}}\|$, is depicted in Fig. 3. While the non-dimensional term $\widetilde{\boldsymbol{o}}$ is directly used in the control, it is not a clear measure for a reader to understand. Therefore, Fig. 4 shows the so-called geodesic measure o_g on $SO(3)$ [22]. This is a measure, in radians or degree, expressing the distance of the deviation matrix $\widetilde{\boldsymbol{R}}$ from the identity. Expressing with $\|\cdot\|_F$ the Frobenius norm, the geodesic measure can be computed as $o_g = 1/\sqrt{2}\|\log\widetilde{\boldsymbol{R}}\|_F$. Within the Appendix it is possible to find the relation between $\widetilde{\boldsymbol{R}}$ and $\widetilde{\boldsymbol{o}}$. It is possible to appreciate that the orientation does not recover the error caused by the interaction with the user. This is evident also for the null-space task as in Fig. 5. The robot does not reach again the initial configuration. The inputs supplied to the robot are depicted in Fig. 6.

This case study bolsters the importance of having the $\boldsymbol{\gamma}$ term within the controller. As explained in Section 3.1, such a term is able to reconstruct an estimation of the external forces acting on the structure at the steady state. Without such an information, the controller is not able to recover the external disturbance caused by the interaction and then it is not possible to suitably control the interaction through both a main and a null-space compliant task.

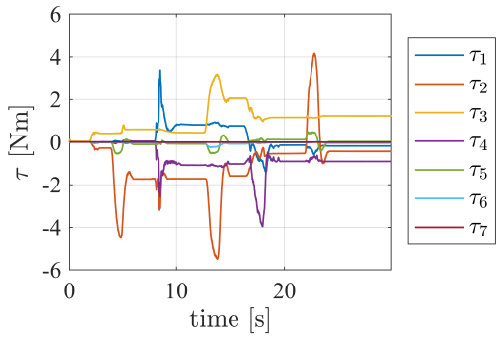

Figure 6: Time history of $\|\boldsymbol{\tau}\|$ for the first case study.

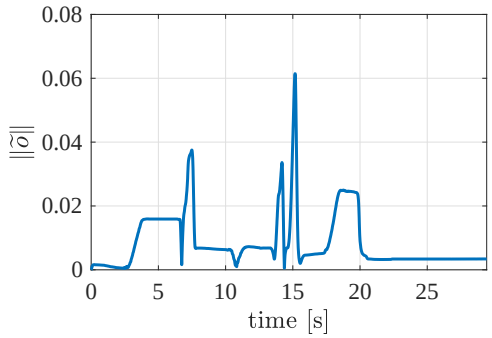

Figure 7: Time history of $\|\widetilde{\boldsymbol{o}}\|$ for the second case study.

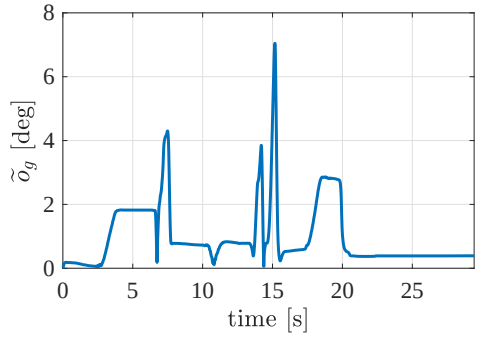

Figure 8: Time history of $\widetilde{o}_g$ for the second case study.

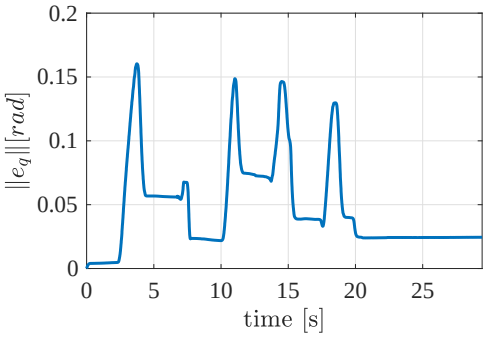

Figure 9: Time history of $\|\boldsymbol{e}_q\|$ for the second case study.

5.2. Case Study 2

In this case study, the whole controller is considered. Time histories of the performed experiments are depicted from Fig. 7 to Fig. 11.

For this case, the deviation of the orientation of Σ_e from the initial configuration, i.e. the time history of $\|\widetilde{\boldsymbol{o}}\|$, is depicted in Fig. 7, while the related geodesic measure is shown in Fig. 8. Now, the norm of the orientation error remains very small for all the duration of the experiment, independently from the occurring contacts with the user with the manipulator. At steady-state, the error norm is about 3.5 $10^{-}3$ rad, that is about 0.2 deg. The error norm does not come back exactly to zero due to the presence of non-negligible joint friction and other small uncertainties that the system is not able to recover.

Regarding the null-space compliant task, the joints configuration error, i.e. the time history of $\|\boldsymbol{e}_q\|$, is shown in Fig. 9. It is possible to appreciate that the manipulator, while it is rigid for the end-effector orientation, is compliant in the rest of its structure. Once each interaction ends, the manipulator recovers the initial configuration. Therefore, also the initial end-effector position is recovered. At steady-state, the joint error norm is about 25 $10^{-}3$ rad, that is about 1.4 deg. The same considerations of above hold.

Finally, the time history of the $\boldsymbol{\gamma}$ term and the manipulator input torques $\boldsymbol{\tau}$ are depicted in Fig. 10 and Fig. 11, respectively.

It is worth pointing out that, since interaction with a human is considered, it is not possible to guarantee a constant $\boldsymbol{\tau}_{ext}$ during the experiments. Even if the developed theory shows asymptotic stability only in case of constant external disturbances, the overall performance remains good.

6. Conclusion

A task space controller based on a singularity free representation for the orientation has been employed in this paper to control a redundant manipulator in the Cartesian space, while achieving a compliant behaviour in the null-space. The designed controller does not need any exteroceptive sensors to accomplish the task, as well as no joints torque sensors are requested. Redundancy is then exploited to ensure a safe physical interaction in case of intentional or unintentional contact with humans, while preserving the main goal at the end-

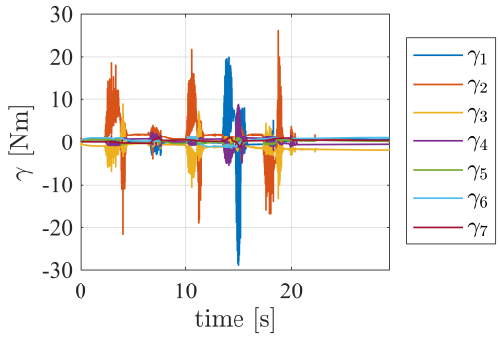

Figure 10: Time history of $\|\boldsymbol{\gamma}\|$ for the second case study.

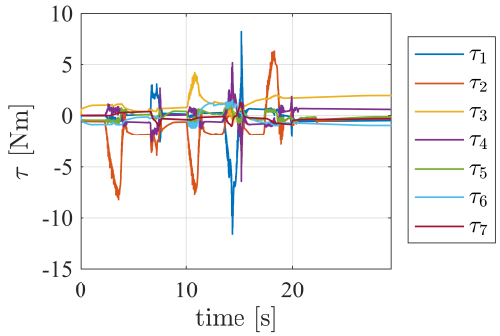

Figure 11: Time history of $\|\boldsymbol{\tau}\|$ for the second case study.

effector with specific reference also to the orientation. Theory and experimental results confirm the effectiveness of the proposed control scheme. As a future work, the tracking problem is the natural evolution of this paper and it is currently under investigation.

Appendix

Angle/axis

The matrix $\widetilde{\boldsymbol{R}}$ can be also seen as a rotation of an angle $\widetilde{\phi} \in \mathbb{R}$ around the unit vector $\widetilde{\boldsymbol{k}} \in \mathbb{R}^3$, such that $\widetilde{\boldsymbol{R}}(\boldsymbol{\alpha}) = \boldsymbol{I}_3 + \sin\widetilde{\phi}\boldsymbol{S}(\widetilde{\boldsymbol{k}}) + (1-\cos\widetilde{\phi})\boldsymbol{S}(\widetilde{\boldsymbol{k}})^2$, with $\boldsymbol{\alpha} = \begin{bmatrix}\widetilde{\phi} & \widetilde{\boldsymbol{k}}^{\mathrm{T}}\end{bmatrix}^{\mathrm{T}}$, and where $\boldsymbol{S}(\cdot) \in \mathbb{R}^3$ is the skew-symmetric matrix. The angle is taken to be positive counter-clockwise about the axis $\widetilde{\boldsymbol{k}}$. Notice that such representation is not unique, since $\widetilde{\boldsymbol{R}}(\widetilde{\phi}, \widetilde{\boldsymbol{k}}) = \widetilde{\boldsymbol{R}}(-\widetilde{\phi}, -\widetilde{\boldsymbol{k}})$.

Expressing the columns of the current and desired rotation matrix of Σ_e with respect to Σ_i as $\boldsymbol{R}_e = \begin{bmatrix}\boldsymbol{n}_e & \boldsymbol{s}_e & \boldsymbol{a}_e\end{bmatrix}$ and $\boldsymbol{R}_d = \begin{bmatrix}\boldsymbol{n}_d & \boldsymbol{s}_d & \boldsymbol{a}_d\end{bmatrix}$, respectively, it is possible to choose the following expression for the orientation error [8]

$$\begin{aligned}\widetilde{\boldsymbol{o}} &= \boldsymbol{f}_o(\boldsymbol{\alpha}) \\ &= \frac{1}{2}\left(\boldsymbol{S}(\boldsymbol{n}_e)\boldsymbol{n}_d + \boldsymbol{S}(\boldsymbol{s}_e)\boldsymbol{s}_d + \boldsymbol{S}(\boldsymbol{a}_e)\boldsymbol{a}_d\right).\end{aligned} \tag{25}$$

The error in (25) is zero when $\widetilde{\boldsymbol{R}} = \boldsymbol{I}_3$, that is the axes of $\boldsymbol{R}_d$ and $\boldsymbol{R}_e$ are aligned as desired, and thus $\boldsymbol{n}_d = \boldsymbol{n}_e$, $\boldsymbol{s}_d = \boldsymbol{s}_e$ and $\boldsymbol{a}_d = \boldsymbol{a}_e$. Moreover, given $\boldsymbol{\omega}_d = \boldsymbol{0}_3$ as in the assumptions of Proposition 1, it is possible to show that (20) holds with

$$\begin{aligned}\boldsymbol{L}(\boldsymbol{\alpha}) = \frac{1}{2}\big(&\boldsymbol{S}(\boldsymbol{n}_d)\boldsymbol{S}(\boldsymbol{n}_e) + \boldsymbol{S}(\boldsymbol{s}_d)\boldsymbol{S}(\boldsymbol{s}_e) \\ &+ \boldsymbol{S}(\boldsymbol{a}_d)\boldsymbol{S}(\boldsymbol{a}_e)\big).\end{aligned} \tag{26}$$

Such a matrix is invertible as specified in [8]. Finally, it is possible to choose $\boldsymbol{K}_o = \boldsymbol{L}(\boldsymbol{\alpha})^{\mathrm{T}}$ and $\boldsymbol{K}_{V,2} = \boldsymbol{I}_3$. This allows to set $f_V = 0$, for which it is straightforward to verify (19).

Unit quaternion

Some drawbacks of the angle/axis representation can be overcome by the *unit quaternion*. This is a parameterization of the rotation matrix $\widetilde{\boldsymbol{R}}$ such that

$$\widetilde{\eta} = \cos\left(\frac{\widetilde{\phi}}{2}\right), \tag{27}$$

$$\widetilde{\boldsymbol{\epsilon}} = \sin\left(\frac{\widetilde{\phi}}{2}\right)\widetilde{\boldsymbol{k}}, \tag{28}$$

where $\widetilde{\boldsymbol{\epsilon}} \in \mathbb{R}^3$ is called *angular part* of the quaternion, while $\widetilde{\eta} \in \mathbb{R}$ is its *scalar part*. The quaternion is termed unit since it satisfies the following constraint $\widetilde{\boldsymbol{\epsilon}}^{\mathrm{T}}\widetilde{\boldsymbol{\epsilon}} + \widetilde{\eta}^2 = 1$. Therefore, it is possible to write $\widetilde{\boldsymbol{R}}(\boldsymbol{\alpha}) = \left(\widetilde{\eta}^2 - \widetilde{\boldsymbol{\epsilon}}^{\mathrm{T}}\widetilde{\boldsymbol{\epsilon}}\right)\boldsymbol{I}_3 + 2\widetilde{\boldsymbol{\epsilon}}\widetilde{\boldsymbol{\epsilon}}^{\mathrm{T}} + 2\widetilde{\eta}\boldsymbol{S}(\widetilde{\boldsymbol{\epsilon}})$, where $\boldsymbol{\alpha} = \begin{bmatrix}\widetilde{\eta} & \widetilde{\boldsymbol{\epsilon}}^{\mathrm{T}}\end{bmatrix}^{\mathrm{T}}$. Notice that the quaternion space is a double cover of $SO(3)$, since it can be seen that $(\widetilde{\eta}, \widetilde{\boldsymbol{\epsilon}})$ and $(-\widetilde{\eta}, -\widetilde{\boldsymbol{\epsilon}})$ corresponds to the same rotation matrix. Also notice that $\widetilde{\boldsymbol{\epsilon}} = \boldsymbol{0}_3$ if and only if $\widetilde{\eta} = \pm 1$. Then $(\widetilde{\eta} = 1, \widetilde{\epsilon} = \boldsymbol{0}_3)$ and $(\widetilde{\eta} = -1, \widetilde{\boldsymbol{\epsilon}} = \boldsymbol{0}_3)$ correspond to $\widetilde{\boldsymbol{R}} = \boldsymbol{I}_3$, and thus $\boldsymbol{R}_e = \boldsymbol{R}_d$ as desired. Therefore, it is possible to specify the orientation error as

$$\widetilde{\boldsymbol{o}} = \boldsymbol{f}_o(\boldsymbol{\alpha}) = \widetilde{\boldsymbol{\epsilon}} \tag{29}$$

for the unit quaternion representation. Moreover, the following kinematic equations for the quater-

nion hold

$$\dot{\widetilde{\eta}} = -\frac{1}{2}\widetilde{\boldsymbol{\epsilon}}^{\mathrm{T}}\widetilde{\boldsymbol{\omega}}, \tag{30a}$$

$$\dot{\widetilde{\boldsymbol{\epsilon}}} = \frac{1}{2}\left(\widetilde{\eta}\boldsymbol{I}_3 + \boldsymbol{S}(\widetilde{\boldsymbol{\epsilon}})\right)\widetilde{\boldsymbol{\omega}}. \tag{30b}$$

Observing (30b), the matrix $\boldsymbol{L}(\boldsymbol{\alpha})$ in (20) can thus be defined as

$$\boldsymbol{L}(\boldsymbol{\alpha}) = \frac{1}{2}\left(\widetilde{\eta}\boldsymbol{I}_3 + \boldsymbol{S}(\widetilde{\boldsymbol{\epsilon}})\right) \tag{31}$$

for the unit quaternion representation. Due to its structure, it is straightforward to show that such a matrix is always invertible. Finally, it is possible to choose $\boldsymbol{K}_o = k_\epsilon \boldsymbol{I}_3$, with $k_\epsilon > 0$ and $\boldsymbol{K}_{V,2} = 2k_\epsilon \boldsymbol{I}_3$. This allows to set $f_V = k_\epsilon(\widetilde{\eta}-1)^2$, for which, given (30),it is possible to verify (19). Notice that, when $\widetilde{\boldsymbol{o}} = \widetilde{\boldsymbol{\epsilon}} = \boldsymbol{0}_3$, the indetermination $\widetilde{\eta} = \pm 1$ does not affect the system stability [17].

Acknowledgements

The research leading to these results has been supported by the RoDyMan project, which has received funding from the European Research Council FP7 Ideas under Advanced Grant agreement number 320992. The authors are solely responsible for the content of this manuscript.

References

[1] H. Sadeghian, L. Villani, M. Keshmiri, B. Siciliano, Task-space control of robot manipulators with null-space compliance, IEEE Transactions on Robotics 30 (2) (2014) 493–506.

[2] D. Kulic, E. Croft, Pre-collision safety strategies for human-robot interaction, Autonomous Robots 22 (2) (2007) 149–164.

[3] A. Cirillo, F. Ficuciello, C. Natale, S. Pirozzi, L. Villani, A conformable force/tactile skin for physical human-robot interaction, IEEE Robotics and Automation Letters 1 (1) (2015) 41–48.

[4] S. Haddadin, A. Albu-Schaffer, A. De Luca, G. Hirzinger, Collision detection and reaction: A contribution to safe physical human-robot interaction, in: 2008 IEEE/RSJ International Conference on Intelligent Robots and Systems, Nice, F, 2008, pp. 3356–3363.

[5] A. Smith, F. Mobasser, K. Hashtrudi-Zaad, Neural-netweork-based contact force observers for haptic applications, IEEE Transactions on Robotics 22 (6) (2006) 1163–1175.

[6] A. De Luca, A. Albu-Schaffer, S. Haddadin, G. Hirzinger, Collision detection and safe reaction with the DLR-III lightweight robot arm, in: 2006 IEEE/RSJ International Conference on Intelligent Robots Systems, Beijing, C, 2006, pp. 1623–1630.

[7] A. Bicchi, G. Tonietti, Fast and soft arm tactics: Dealing with the safety performance trade-off in robot arms design and control, IEEE Robotics and Automation Magazine 11 (2) (2004) 22–33.

[8] B. Siciliano, L. Sciavicco, L. Villani, G. Oriolo, Robotics: Modelling, Planning and Control, Springer, London, UK, 2009.

[9] N. Hogan, Impedance control: An approach to manipulation: Parts I–III, ASME Journal of Dynamic Systems, Measurement, and Control 107 (2) (1985) 1–24.

[10] C. Ott, Control of nonprehensile manipulation, in: Cartesian impedance control of redundant and flexible joint robots, Vol. 49 of Springer Tracts in Advanced Robotics, Springer, New York, NY, USA, 2008.

[11] F. Ficuciello, L. Villani, B. Siciliano, Variable impedance control of redundant manipulators for intuitive human-robot physical interaction, IEEE Transactions on Robotics 31 (4) (2015) 850–863.

[12] H. Sadeghian, L. Villani, M. Keshmiri, B. Siciliano, Multi-priority control in redundant robotic systems, in: 2011 IEEE/RSJ International Conference on Intelligent Robots and Systems, San Francisco, CA, USA, 2011, pp. 3752–3757.

[13] O. Maaroof, M. Dede, Physical human-robot interaction: Increasing safety by robot arms posture optimization, in: ROMANSY 21 - Robot Design, Dynamics and Control, Vol. 569 of CISM International Centre for Mechanical Sciences (Courses and Lectures), Springer, Cham, 2016.

[14] O. Khatib, L. Sentis, J. Park, J. Warren, Whole-body dynamic behavior and control of human-like robots, International Journal of Humanoid Robotics 1 (2004) 29–43.

[15] W. Oh, Y. nad Chung, Y. Youm, Extended impedance control of redundant manipulators based on weighted decomposition of joint space, Journal of Intelligent and Robotic Systems 15 (5) (1998) 231–258.

[16] O. Khatib, Inertial properties in robotic manipulation: An object-level framework, International Jorunal of Robotics Research 14 (1) (1995) 19–36.

[17] F. Caccavale, C. Natale, B. Siciliano, L. Villani, Resolved-acceleration control of robot manipulators: A critical review with experiments, Robotica 16 (1998) 565–573.

[18] A. De Luca, G. Oriolo, Nonholonomic behavior in redundant robots under kinematic control, IEEE Transactions on Robotics and Automation 13 (5) (1997) 776–782.

[19] C. Ott, A. Kugi, Y. Nakamura, Resolving the problem of non-integrability of null-space velocities for compliance control of redundant manipulators by using semi-definite lyapunov functions, in: 2008 IEEE International Conference on Robotics and Automation, Pasadena, CA, USA, 2008, pp. 1999–2004.

[20] A. Iggidr, G. Sallet, On the stability of nonautonomous systems, Automatica 39 (2003) 167–171.

[21] G. Schreiber, A. Stemmer, R. Bischoff, The fast research interface for the KUKA lightweight robot, in: 2010 IEEE International Conference on Robotics and Automation, Workshop on Innovative Robot Control Architectures for Demanding (Research) Applications, Anchorage, AK, USA, 2010, pp. 15–21.

[22] D. Huynh, Metrics for 3D rotations: Comparison and analysis, Journal of Mathematical Imaging and Vision 35 (2009) 155–164.